Chapter 2

Techniques of Radio Interferometry

2.1 Introduction

A very useful tracer of the atomic phase of ISM is the 21-cm line. The emission and absorption of this line can be traced using observations by radio telescopes. At radio wavelengths, the angular resolution $\delta\theta = 1.22\lambda/D$ of a single-dish radio telescope is very poor as it is directly proportional to the wavelength λ and inversely proportional to the dish diameter D. For example, the single-dish radio telescope having maximum diameter is Five hundred meter Aperture Spherical Telescope (FAST). Its resolution at 21 cm $\sim 1.7'$, not enough to study any small scale structure at radio wavelengths. This limitation of the single-dish radio telescope makes it very difficult to study any small scale Galactic structure. It can be avoided by increasing the dish size of the telescope to multiple times the diameter of the typical dishes used in the observations at infrared and optical bands. However, making the dish size of a very large diameter is practically not possible. To overcome this problem, a very novel method is used called aperture synthesis. The aperture synthesis technique is based on radio interferometry. In this technique, many single-dish radio telescopes are combined to act as a single radio telescope of a large dish, having an excellent resolution. The achieved resolution in this way is $\sim \lambda/B_{max}$, where B_{max}

is the longest baseline or the largest projected separation between antenna pairs along the direction of the source (in the sky plane), in units of observed wavelengths. Radio interferometers like the GMRT have angular resolutions of about one arc second at the 21-cm wavelengths. This makes the interferometers as telescope of choice for the project.

2.2 Radio Interferometers

Van Cittert–Zernike theorem

The basic component of the radio interferometers is the radio antenna. In most of the modern radio telescopes, parabolic antennas work as radio reflectors to reflect the incoming radio signals on a single point called focus, connected to a receiver. With the help of the signal processing amplifier and modern technologies, the very weak radio signals from the sky are detected. If an antenna of the interferometer is pointed toward a source in the sky whose intensity is $I(\nu,\theta,\phi)$ (Jansky/steradian), then the radiation power received by the antenna in the units of $watt/m^2$ is given as

$$P = A(\nu,\theta,\phi)I(\nu,\theta,\phi)d\nu d\Omega \tag{2.1}$$

Here ν,θ, and ϕ represent the frequency of the observation and pointing direction in the sky, respectively. Independently, θ and ϕ are noted as elevation and azimuthal angle. $d\nu$ and $d\Omega$ are the bandwidth of the observation and the solid angle subtended on the source by the antenna. $A(\nu,\theta,\phi)$ in the above equation represents the reception pattern of the antenna. The dependence of the $A(\nu,\theta,\phi)$ on θ and ϕ shows that the antenna reception pattern is anisotropic and it has the maximum response in some particular direction (toward pointing) in comparison to the other direction. In the interferometers, the position of the antennas may be fixed, or there may be a facility to move antennas from one point to the other so that they could be arranged in a particular way (called configuration) in a

limited range of distance for specific observations. Very Large Array (VLA) consists 27 antennas and has a facility to arrange them at particular positions, making VLA available in many configurations. The interferometer configurations provide unique benefits and make them flexible for scientific purposes with resolutions to study the small scale and the large scale structures. The fixed antenna configuration interferometers like Giant Metrewave Radio Telescope (GMRT) are made so that even their antennas can not be shifted from one position to another, but its configuration allows it to be used for most of the scientific purposes in the same way as VLA like interferometers do. The GMRT has 30 fully steerable antennas with 14 of them in a compact configuration within one square kilometer area. Rest of its antenna are distributed in a Y shaped array. The distribution of GMRT antennas can be seen in figure 2.1. Each pairs of the antenna in a interferometer measures the Fourier transform of the sky intensity $I(\vec{\theta},\nu)$, called visibility function $V(\vec{U},\nu)$. The three-dimensional equation relating to the sky intensity distributions $I(l,m,n)$ and coherence function $V(u,v,w)$ can be written with the help of the Van Cittert–Zernike theorem as

$$V(u,v,w) = \int\int I(l,m,n)e^{-2\pi i(lu+mv+nw)}\frac{dldm}{\sqrt{1-l^2-m^2}} \tag{2.2}$$

Here (u,v,w) are the components of the baseline vector $\vec{U}$ and (l,m,n) are the direction cosines associated with $\vec{\theta}$. For the interferometers where primary beam is < 1 degree, $\sqrt{1-l^2-m^2} \approx 1$ and above equation reduces to

$$\tilde{V}(u,v) = \int\int I(l,m)e^{-2\pi i(lu+mv)}dldm \tag{2.3}$$

where $\tilde{V}(u,v) = e^{2\pi imw}V(u,v,w)$. In the vector form we write above equation as

$$V(\vec{U},\nu) = \int\int d\vec{\theta}e^{-2\pi i\vec{U}.\vec{\theta}}I(\vec{\theta},\nu) \tag{2.4}$$

Here $\vec{U}$ and $\vec{\theta}$ are now two-dimensional vector. Hence for the small field of view, the visibility function is a two-dimensional Fourier transform of the sky brightness distribution. The above equation is valid for the small part of the sky. An interferometer having N antenna in it samples ${}^{N}C_2$ visibilities in a baseline plane at a time. As the source rises in the sky, due to the rotation of the earth, more and more components of the visibilities are sampled, and after few hours of the observation, the baseline plane is filled with visibilities. This is called earth rotation aperture synthesis, as because of the earth rotation, we have well-sampled visibilities in the baseline plane. Later, through the Fourier transform and deconvolution process, the sky brightness is recovered from these observed visibilities. The interferometric field of view is given by the $\sim \lambda/D$, where D is the dish size of the single antenna in the interferometer.

Array configuration and sampling

As mentioned earlier, for an interferometer, the arrangement of the antennas at different locations in a specific manner is called its configuration. Here we discuss some different types of interferometers and their configurations in very short. One of the most sensitive radio interferometer involved in the frontier research in astronomy and astrophysics is Very Large Array (VLA), situated in Socorro, U.S. (Thompson et al., 1980). VLA has 27 operating antennas (each having 25 meters dish size) in a single array, operating in four basic configurations known as A, B, C, and D configurations. Among these configurations, A has the largest baseline (i.e. best resolution), and configuration D has the shortest baseline (minimum resolution). The other configurations B and C have the resolution between configurations A and D. The maximum antenna separations for VLA configurations A, B, C and D are 36.4, 11.1 3.4, and 1.03 km, respectively. VLA has continuous frequency coverage from 1 to 50GHz in the different bands known as L, S, C, X, Ku, K, Ka and Q bands. Here L band covers 1-2GHz. The use of the particular configuration in the

observation is based on the requirement of the resolution, sensitivity, and flux density consideration of the scientific goal. One of the other types of synthesis radio telescope whose antennas can be placed from one position to the other is the Westerbork Synthesis Radio Telescope (WSRT) in the northeastern Netherland. The WSRT is a linear array and consists 14 antennas, 10 of which are fixed, while four are shiftable on rail track giving the maximum baseline of up to 2.7 km. WSRT has an equatorial mount in the east-west line. This type of arrangement makes it to study the exceptional kind of science like polarized emission research as they have a constant orientation toward the sky during observation. Like VLA, WSRT also has configurations known as A, B, C, D, and E to observe in the 310-8650MHz frequency range divided into many bands. Gaint Meterwave Radio Telescope (GMRT) (Swarup et al., 1991) is also one of the very sensitive interferometers situated near the Pune city in (Maharastra state) India. It has 30 antennas, each having 45 m dish size in diameter, 14 of which are in the central region within $\sim$ 1.1 km, and the rest are arranged in a Y shape to provide the maximum resolution of $\sim$ 25 km at a given λ. The locations of the GMRT antennas can be seen in figure 2.1.

The Hybrid configuration of the GMRT makes it suitable to study both small and large scale structures with reliable sensitivity and resolution. GMRT operates in discrete frequency bands: 130-170MHz, 225-245MHz,300-360MHz, 580-660MHz and 1000-1450 MHz. One of the wide-field arrays that use the phased tiles (dual-polarization dipole antennas) for the observation is the Murchison Widefield Array (MWA) (Bowman et al., 2013) , which started its observation nearly a decades ago, situated in Western Australia. MWA is the first step toward making the world's most giant radio telescope, Square Kilometer Array (SKA). At present, it has 128 tiles. MWA is also a static antenna array, like GMRT. Most of the tiles in the MWA are within 1.5 km, called the core region, and they provide very high imaging quality. Few of its antennas are outside the core region to provide the maximum baseline up to 6 km. Each of the radio array discussed above

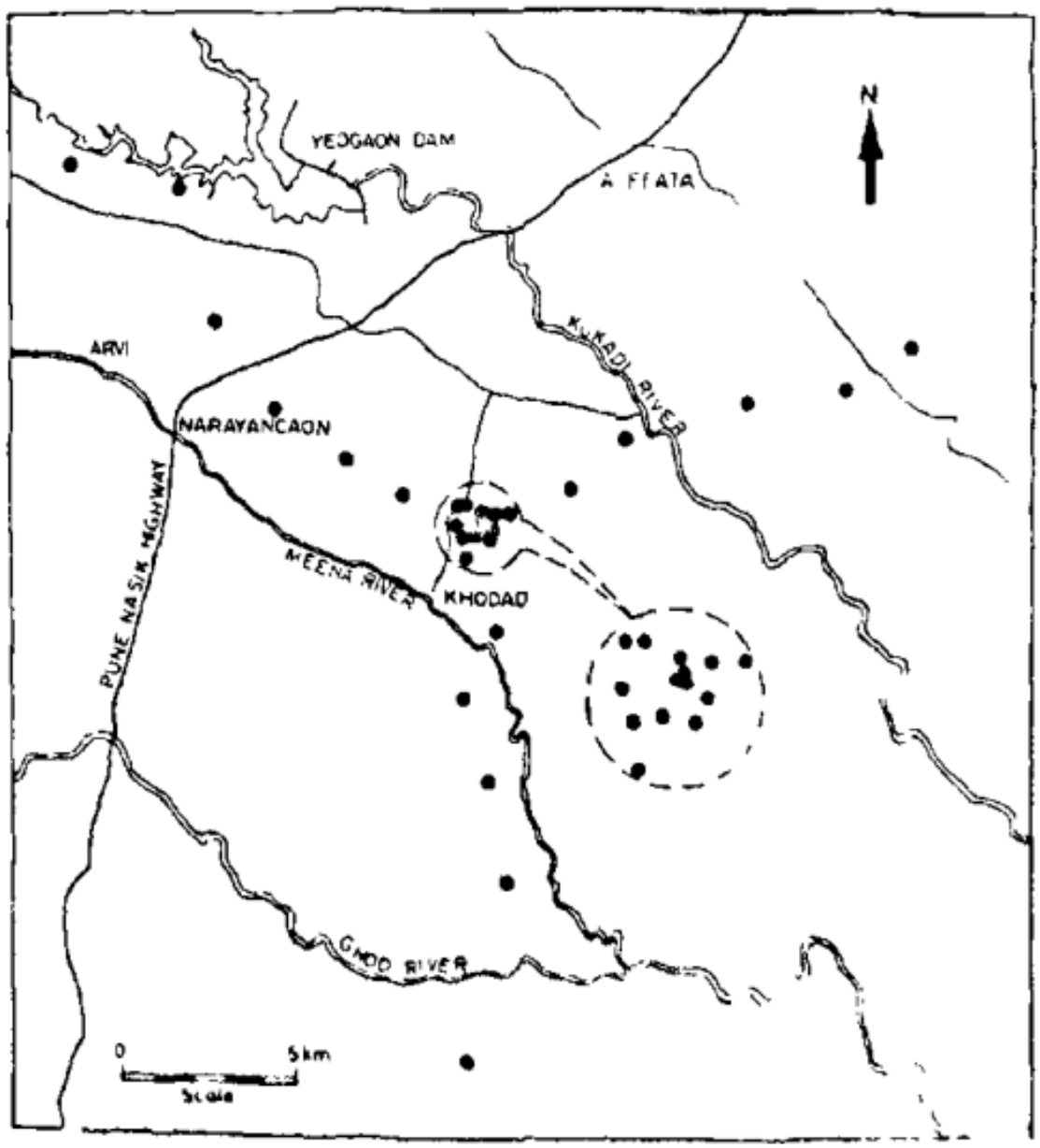

Fig. 2.1 : Image shows the GMRT antenna positions, taken from Swarup et al. (1991). The dot points inside the zoomed circle are the central part of the GMRT consisting 14 antennas.

is designed under a specific model to best suit a scientific goal and observations. For example, MWA is designed to operate at a low-frequency range (70-300MHz) to detect the neutral atomic hydrogen emission from the Epoch of Reionization (EoR), solar burst, and the radio transient phenomenon. WSRT, due to its model and equatorial mount, is best to study the polarized emission observations. The GMRT and VLA's hybrid configurations make it possible to study the very wide range of astrophysical phenomena and events, including Galaxy, astronomical objects, quasars, radio galaxies, supernovae remnants, pulsars, sun, H I component of the galactic ISM, etc. In our study of the scale dependence of the optical depth fluctuations, we would like to use frequency channels with the average optical depth of order unity to get maximum signal to noise in optical depth. Furthermore, the fluctuations of optical depth in these channels need to be measured with more than 3σ significance. The upgraded GMRT has very high velocity resolution (below 0.5km/s) to resolve the fine absorption components of 21-cm and very high sensitivity ($\sim 45\mu Jy$, see Gupta et al. (2017)). With such a high sensitivity, only a few hours of observation on the target source is required to achieve fair signal to noise at the optical depth of unity. Our required resolution for subparsec structures is $\sim 40K\lambda$, which falls within the maximum resolution ($\sim 120K\lambda$) in the L band (1000-1450 MHz) of the GMRT, so we use this interferometer for observations of our target source whenever required.

Instrumental effect

The equation 2.4, representing the visibility $V(\vec{U},\nu)$ as a Fourier transform of the sky brightness and free from any external effect, signifies the true visibility. The measured visibility in the antenna pairs is written as $V_{ij}(t,\nu)$, here i and j represent the antenna indexes. In reality, this observed visibility is corrupted by the instrumental effect and phase disruption as radio waves travel through the ionosphere. Relation between the measured visibility $\tilde{V}_{ij}(t,\nu)$ and the true visibility $V_{ij}(t,\nu)$ in a very simplified form can be written

as

$$\tilde{V}_{ij}(t,\nu) = G_{ij}(t,\nu)V_{ij}(t,\nu) \tag{2.5}$$

Here $G_{ij}(t,\nu)$ represents the baseline based complex gain between the antenna pair i, j. The baseline based complex gains $G_{ij}(t,\nu)$ can be decomposed in terms of the antenna-based complex gains as

$$G_{ij}(t,\nu) = g_i(t,\nu)g_j^*(t,\nu) \tag{2.6}$$

The time-dependent part in the gain mostly comes from the antenna and ionosphere, while the frequency-dependent gain is the result of the bandpass response. The ionosphere corrupts the observed visibility phase by introducing an excess path length in the radio waves as it propagates through it.

2.3 Data analysis methodologies

Calibration

Observation of a source with an interferometer gives us the Fourier transform of the sky brightness toward the source in the form of visibilities. In a single integration time, a radio interferometer having N element (antenna) in it, samples ${}^{N}C_2$ visibilities corrupted with the instrumental noise, gain and phase disruption, and it requires the correction of its phase and amplitude before the data is used for any scientific purpose. This process of recovering the corrupted visibility to make it almost like true visibility is known as calibration. As the number of observed visibilities in the baseline pairs is larger than the antenna numbers, the antenna-based gain can be solved from the baseline-based gains. This correction is achieved with the help of the flux, phase, and bandpass calibrators observed along with the target source. This requires calibrators to be observed with a strategy mentioned below.
The flux calibrators are generally a strong point source of known flux density and are

used to solve the amplitude part of the antenna gain. They are generally observed at the beginning and end of the observation for few minutes. In the observation, if the same flux calibrator is not available till the end, then another flux calibrator may also be observed at the end of the observation. The observation of the phase calibrator requires it to be near the target source so that the phase corruption that happened due to the same part of the ionosphere could be properly corrected. Phase calibrators are also chosen to be a point source so that the changes produced in the phase by the ionosphere is easily noted. During the observation, both the target source and the phase calibrator are observed alternatively for many times as phase changes due to the ionosphere may happen quickly. Each time phase calibrator is observed for a few minutes while the time for the target source is several times to those of the phase calibrator. To correct for the frequency dependence gain, bandpass calibrators are used. We choose the bandpass calibrators to those sources whose frequency response is well known across the observation bandwidth. The bandpass calibrators are chosen such that they don't have any spectral features across the band, and their frequency dependence across the band is well known and are bright enough to produce bandpass gains of signal to noise ≥ 5. Bandpass calibrators are neither required to be near the target source, nor are they required to be a point source, and they are also observed on the same time scale as flux calibrators. When the bandpass calibrators are not available, the frequency switching technique on the phase calibrator is applied to serve it as a bandpass calibrator. Bandpass calibrators are also preferred to be observed at the beginning and end of the observations. The observation strategy of the calibrators is shown in figure 2.2.

The process of calibration consists of carrying out the primary calibration and self-calibration.

- **Primary Calibration**: In the primary calibration, first, we set the flux scale of the flux calibrator. At the very basic level, we calibrate the single channel of both flux

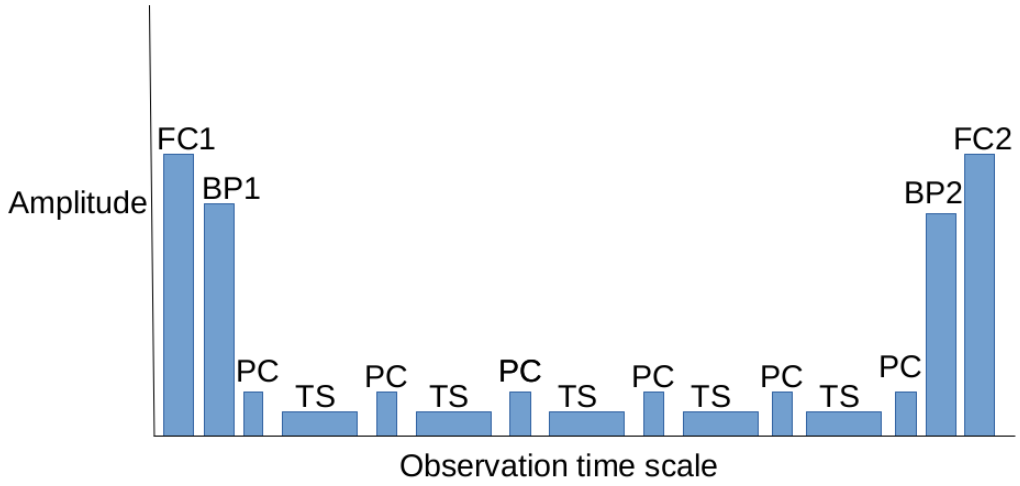

Fig. 2.2 : The above figure shows the observation strategy of a target source along with calibrators. Flux Calibrators (FC1 and FC2) and Bandpass Calibrators (BP1 and BP2) are observed at the beginning and end, while Phase Calibrator (PC) and Target source (TS) are observed alternatively.

and phase calibrators and ensure that we have identified and flagged the data points coming from the bad antenna and bad time intervals in the observation that must not go in the next stage of the calibration. The same thing is done for the bandpass calibrators too. We correct the amplitude and phase of the single-channel target source using the prepared single-chain gain tables of the phase and flux calibrators. Here we note and flag the bad baselines of the visibility data in the target source too. Once we have identified and flagged the globally known bad data from the calibrators and target source, we move to the next primary calibration stage. Using the single-channel gain solution, we solve for frequency-dependent gains across the whole frequency range (channels), called bandpass solution. Now using these tables of the frequency response across the band, the amplitude and phase correction tables of the flux and phase calibrators are prepared. At the final stage, a flux scaling table is made to scale the amplitudes of the phase calibrator and target source, which were set to unity before the calibration. Finally, we use these prepared tables of the phase

solution, amplitude gain, and bandpass solution on the flux and phase calibrators across all the channels to take care of the phase, amplitude, and bandpass correction. We now search the remaining bad data across the channels and flag them. After ensuring that there are no more bad visibilities, we again make the calibration tables using this flagged visibility data and finally apply it to the target source. We search the bad visibility data in the target source for the final stage; if any bad data is found, we flag them before it is used for self-calibration or any scientific purpose.

- **Self Calibration**: In the calibration with observed calibrators, gains are interpolated for the intermediate and unknown values of time-dependent gains i.e. antenna gains are not properly determined at each timestamp of observation, but they are interpolated. Because of this, the quality of the final deconvolved image suffers from artifacts and other systematical errors. To minimize such an error self-calibration technique is used. In this technique, antenna gains are determined, which minimizes the difference between model visibilities and observed visibilities. For the extended source, the model visibilities is generally determined by CLEAN task, which is used to construct the image. The process of self-calibration is an iterative process to determine the better model at each time. In the first stage, phase-only self-calibration is performed, followed by phase and amplitude calibration. For self-calibration to work properly, the signal to noise is preferred to be ~ 5 or even larger at each baseline. Self-calibration, if guided in the proper way, can improve the signal to noise in a significant manner.

We do these calibration processes in the Common Astronomical Software Application (CASA) (McMullin et al., 2007). To set the flux density of the flux calibrator *setjy* task is used. For pre-phase calibration, delay calibration, amplitude-phase calibration a common task *gaincal* can be used. For the bandpass calibration and preparation of the flux scaling,

bandpass and *fluxscale* tasks are respectively used. To apply the calibration tables on the target source and the calibrators, task *applycal* is implemented in the CASA.

Imaging

The observed visibilities by the interferometers are the function of the baseline vector $\vec{U}$ formed between the antenna pairs. Since the antennas have a discrete location, the observed visibilities are sampled discretely. The sampling function for the visibilities can be defined as

$$S(\vec{U}) = \sum \delta_D(\vec{U} - \vec{U}_i) \tag{2.7}$$

Here $\vec{U}_i$ represents the discrete baseline formed by the antenna pairs in the interferometer, and $\sum$ runs over the total number of observed baselines. So the sampled visibilities are given as

$$V^s(\vec{U}) = \sum \delta_D(\vec{U} - \vec{U}_i) V(\vec{U}) \tag{2.8}$$

For simplicity, here, we have avoided writing visibility as a function of time and frequency. The Fourier transform of this sampled visibility is called the dirty image I^D, which is

$$I^D(\vec{\theta}) = \mathscr{F}S(\vec{U}) \otimes \mathscr{F}V(\vec{U}) \tag{2.9}$$

Here $\otimes$ represent the convolution and $\mathscr{F}$ stands as a sign of the Fourier transform. Fourier transform of a function $u(t)$ is defined as

$$\mathscr{F}[u(t)] = \int_{-\infty}^{\infty} u(t) e^{-2\pi i k t} dt \tag{2.10}$$

Here k is the Fourier conjugate of t. Hence equation 2.9 also can be written as

$$I^D(\vec{\theta},\nu) = I(\vec{\theta},\nu) \otimes B_D(\vec{\theta}) \tag{2.11}$$

$B_D(\vec{\theta})$ is the Fourier transform of the $S(\vec{U})$ and represent the dirty beam (PSF) of the interferometer.

- **Dirty image**: In the interferometric imaging, Fourier inversion of observed visibilities produce an image called the dirty image. This dirty image results from the convolution between the Fourier transforms of sampling function and the so-called continuous visibility function measurement, as given in equation 2.8.

- **Deconvolution**: To get the high-quality radio interferometric image from the dirty image, we need to deconvolve the dirty beam from the dirty image. The two basic methods that are used for this work are, 1) CLEAN and 2) Maximum Entropy Method (MEM). Here we first describe the CLEAN and then will describe MEM in very short.

  1] CLEAN: CLEAN is a non-linear deconvolution method to reconstruct the sky brightness from the dirty image I^D. Many algorithms are used for the this deconvolution process, and few of them are implemented in the CASA as the task "CLEAN" (see Högbom (1974), Cotton (1979), Clark (1980), Schwab (1984)). In the CLEAN algorithm, the sky is treated as the collection of the point sources. This algorithm first makes the dirty image from the visibility data using the Fast Fourier Transform (FFT) before it proceeds for the deconvolution process. Since the visibility data are not sampled uniformly in the baseline plane; hence gridding is used to interpolate the visibilities in regular intervals so that FFT could be performed to produce $I^D(\vec{\theta})$. To

control the beam shape and suppress the unnecessary sidelobes outsides the central maxima, weighting functions are used. Weighting includes tapering the visibility data outside some baseline range as well as locally averaging it. The two most commonly used weighting schemes are natural weighting and uniform weighting. Natural weighting provides the same weight to all measured visibilities, while in uniform weighting, visibilities are weighted by their local average. Natural weighting provides the wider PSF, while uniform weighting provides the narrower one. After constructing the dirty image and PSF, CLEAN progresses in the following manner,

i) Strength and position of the brightest point are searched in the image.

ii) From the peak position, a product of the dirty beam, peak strength, and loop gain (user-defined) is subtracted, and this magnitude and the position of the substracted point source is recorded in a model.

iii) Go to step (i) and continue this loop until a threshold is reached (user-specified), below which the peaks are treated as residuals.

iv) Convolve the accumulated point source with a CLEAN beam (generally elliptical gaussian).

v) Finally, add the residual in this convolved image.

After step number (v) we get a final deconvolved image which is called the CLEANed image. The theoretical sensitivity of a image outside the source in Jy/beam unit is given as

$$\sigma_I = \frac{T_{sys}}{G\sqrt{N_b N_{pol} d\nu t_{int}}} \tag{2.12}$$

Here T_{sys}, G, N_b, N_{pol} , t_{int} are the system temperatue (K), per antenna gain (K/Jy/Antenna), no of baselines, no of polarizations and integration time respectively. The system temprature constitute contributions from reciever temprature T_R, off Galactic sky plane temprature T_{sky} and typical ground temprature T_{ground}. The noise in the image by natural weighting is always less than those of the uniform

weighting. Although the CLEAN algorithm is very efficient and useful, it still has some limitations,

i) The CLEAN algorithm produces artifacts outside the sources, and it can not be avoided.

ii) For an extended source CLEAN does not produce a unique solution (i.e. a unique image) as the final deconvolved image depends on the loop gain, threshold, weighting schemes etc.

ii) The noise in the output image across the channels may be correlated even though the noise in the visibility across channels may not be correlated.

To avoid any aliasing in the output image, we sample at least two pixels within the resolution. Our study uses the *tclean* task in the CASA tool to produce the CLEANed image. We use Hogbom CLEAN (Högbom, 1974), which is the most favored for the deconvolution of the extended sources like supernova remnants because it does not show any error in the PSF construction.

Other than the CLEAN algorithm, the Maximum Entropy Method (MEM) (Narayan and Nityananda, 1986) is also used to deconvolve the dirty beam from a dirty image. Here we describe MEM in very short.

2] MEM: It is also a powerful method to deconvolve the dirty beam from a dirty image. Here the image is obtained by maximizing the entropy, generally defined as

$$H = -\sum_{k} I_k ln \frac{I_k}{M_k} \tag{2.13}$$

Here I_k is the brightness of the k^{th} pixel and M_k represents some default image. Unlike CLEAN, MEM is not procedural. The MEM has advantages in that it generally works faster than CLEAN.

Spectroscopy

For spectroscopy, continuum and multichannel (cube) radio images are reconstructed to map the spectral features towards the source. The produced cube is a function of the sky direction $\vec{\theta}$ and frequency i.e. $I(\vec{\theta}, \nu)$. This image can be used to measure the radio spectra of the source in the following manner. First, we average $I(\vec{\theta}, \nu)$ along each direction over the face of the source in each channel so that we get the flux as a function of the channel (or frequency). This is called spectra. Now we fit the continuum channels of the spectra with the second-order polynomial. Using the fitted parameters, we correct any undesired spectral feature in the continuum part of spectra and use the fitted 0th order parameter as the mean flux of the source. To achieve the continuum subtracted spectra, we subtract the mean value of the continuum flux from the spectra across the channels. To generate the optical depth map, cube $I(\vec{\theta}, \nu)$ is divided by the continuum map $I_c(\vec{\theta})$ such that

$$\tau(\vec{\theta}, \nu) = -log\left[\frac{I(\vec{\theta}, \nu)}{I_c(\vec{\theta})}\right] \tag{2.14}$$

here $\tau(\vec{\theta}, \nu)$ represents optical depth map of the intervening medium towards the source. Similar to the flux spectra, we may also obtain the optical depth spectra using the same procedure. To construct the cube of the radio image, parameter *mode=cubedata* is used in task CLEAN.